Highly sensitive and homogeneous SERS substrate fabricated by a femtosecond laser combined with dewetting

Xudong Tan (谭旭东), Lan Jiang (姜 澜), Jie Hu (胡 洁)*, Pengjun Liu (刘鹏军), Andong Wang (王安东), and Yong Lu (芦 勇)

Laser Micro/Nano Fabrication Laboratory, School of Mechanical Engineering, Beijing Institute of Technology, Beijing 100081, China

**Corresponding author: jiehu2@bit.edu.cn*

Received June 16, 2015; accepted September 10, 2015; posted online October 5, 2015

We report a simple, cost-effective and repeatable method for fabricating a large area and uniform substrate for surface-enhanced Raman scattering (SERS). The silicon, micromachined by a femtosecond laser, is coated with gold film and then treated through the dewetting process. The morphology shows a higher electric field enhancement due to light trapping. The enhancement factor of the SERS substrate is 9.2×10^7 with a 5 nm-thick film coated. Moreover, it also exhibits a uniform signal through Raman mapping and chemical stability with the greatest intensity deviation of 6% after a month. The proposed technique provides an opportunity to equip microchips with the SERS capabilities of high sensitivity, chemical stability, and homogeneous signals.

OCIS codes: 240.6695, 140.7090.
doi: 10.3788/COL201513.111401.

Since its discovery in 1974 by Fleischmann *et al.*, surface-enhanced Raman scattering (SERS) has been extensively researched in chemistry, biology, and materials sciences[1–5]. The related research field covers the enhancement mechanism of SERS as well as its applications as a sensitive surface analytical tool for chemo/bio sensing[3–5]. The mechanisms of the electromagnetic (EM) enhancement induced by surface plasmon resonance usually require a nanostructured metal substrate where the collective oscillation of the free electrons is confined, leading to localized surface plasmon resonance (LSPR) under irradiation of light[6]. The peak position and intensity of LSPR can be strongly influenced by the roughness of the prepared nanostructures.

Nanostructure plays an important role in producing high-intensity scattering signals because it increases the surface roughness and facilitates the generation of "hot spots" that existed between adjacent nanoparticles (NPs) and greatly enhances the EM field around them. Over the past decade, most SERS substrates have been manufactured by the conventional lithographic method; hence, the development of cost-effective and simple procedures to create nanostructured surfaces is attracting more attention in the SERS research field. The advancement in femtosecond (fs) laser technology has opened new possibilities for cost-effective fabrication of nanostructures on most solid materials[7–12].

More recently, fs laser-irradiated silicon wafers with diverse surface morphologies have been reported to yield high SERS enhancement factors (EFs) when coated with thin film[13] and used in conjunction with methods such as lithography[14] or nanosecond laser processing[15,16]. It has also been demonstrated that the nanostructures formed by the laser processing in silver nitrate solutions can produce high EFs[17–19]. Despite these advantages, in nanosecond laser processing it is often difficult to control the signal homogeneity due to non-uniform thermal effects. In the solution processing system, the suspended silicon debris would disturb further fabrication to form a large and uniform substrate. Moreover, the chemical instability of silver is an intrinsic drawback. Although the EF of gold is not as high as silver, the high chemical stability and molecular compatibility are considerable advantages. Therefore the current demand of reliable and low-cost substrates with both large-scale uniformity and high EFs have severely limited the use of SERS in most applications.

In this Letter, we first propose a two-step approach that effectively combines fs laser fabrication and the thermal dewetting process to obtain a NP array distributed throughout the micro/nano structure, as illustrated in Fig. 1. The first step is to fabricate large and uniform

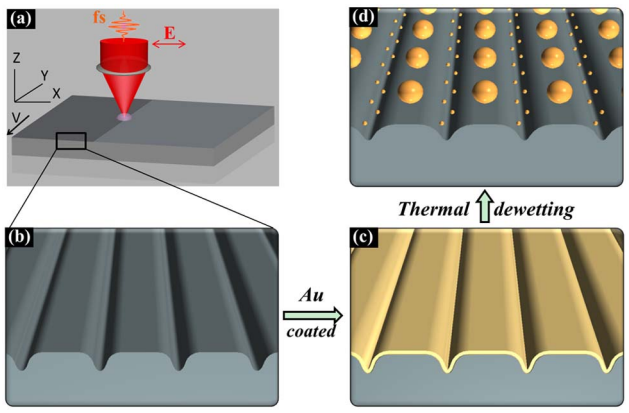

Fig. 1. Schematic fabrication process of SERS substrates.

periodic micro/nano structures on a silicon wafer using a fs laser pulse. Then a 10 nm-thick gold film is coated on the processed substrate by an ion beam sputtering (682, Gatan) method, and a muffle furnace (GHA12/300, Carbolite) is employed to heat the Au-coated substrate for the thermal dewetting. The film thickness can be accurately controlled by the sputtering time. The temperature rise rate is set at 30°C/min and kept at 1000°C for 1 h in order to induce the dewetting. Abundant and uniform Au NPs adhered on machined silicon structure will provide a SERS-active substrate with high sensitivity, chemical stability, and spatially homogeneous signals. The EF of the SERS substrate is measured to be higher than 10^7 and the greatest Raman intensity deviation is estimated to be in the range of 6% for the substrate exposed in the air for a month.

A regenerative Ti-sapphire laser system (800 nm, 35 fs) is used in the experiment to fabricate large-area, uniform-periodic-surface micro/nano structures at ambient temperature. The linearly polarized laser is focused perpendicular to the substrate using an objective lens (Olympus MPLFLN 10×, NA = 0.3). The silicon sample (single-crystal 100-Si wafers) is mounted on a computer-controlled, six-axis translation stage (M-840.5DG, PI, Inc.) with a resolution of 1 μm in the x and y directions and 0.5 μm in the z direction. The laser fluence is adjusted by the combination of an achromatic half-wave plate and a linear polarizer. The silicon sample is cleaned in an ultrasonic bath with acetone for 15 min and then dried in the air at room temperature. High-pressure nitrogen gas is applied to prevent the silicon debris from depositing on the machined region. The fs laser-induced periodic surface structures (LIPSSs, also called ripples) are created by using a laser fluence of 0.30 J/cm^2, a repetition rate of a 1 kHz, and a scan speed of 150 μm/s. The scan direction is perpendicular to the fs laser polarization and the interval is 2 μm so that two adjacent scanning lines can be slightly overlapped in order to form large-area, uniform periodic structures. A uniform and clean area (5000 μm× 100 μm) is generated. Morphological characters are investigated by a scanning electron microscope (SEM) and atomic force microscope (AFM). As shown in Fig. 2, the period width of the ripple is approximately 565 nm and the depth of the groove is approximately 140 nm.

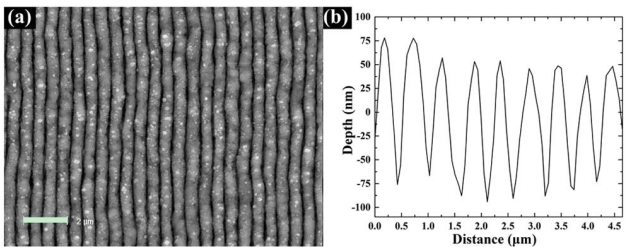

Fig. 2. (a) SEM image and (b) AFM profile of the surface morphology written on silicon samples. The scale bar represents 2 μm.

For comparison purposes, a flat silicon substrate with the same conditions as the 10 nm gold film is also treated with thermal dewetting. The mean particle diameter is 218 nm (standard deviation 51 nm), as shown in Figs. 3(a) and 3(b). In contrast, the ripple structure will affect the formation of Au NPs. It is interesting to note that the coarse NPs are distributed along the ridges and the fine particles are distributed along the trench. The particles have a nearly circular cross section of around 45–55 nm in size, while the coarse particles are often a little elongated along the orientation of the ridges and are ~150–250 nm in size. This clearly indicates that the morphology of the ripple structure strongly affects the NPs formation.

All the prepared substrates are submerged in rhodamine 6G (R6G) solutions to adsorb a single layer of R6G molecules for Raman signal-enhancement tests. Raman spectra are obtained by a Renishaw Raman microscope using a 532 nm He-Ne laser and a maximum exciting power of 40 mW. The grating and objective lens used are 1800 lines/mm and a 50× microscope objective (NA = 0.5), respectively. A concentration of 10^{-2} mol/L of R6G is used for the fs laser-machined Si substrate (reference substrate) and 10^{-6} mol/L for all other substrates. The exciting powers of the SERS-active substrates and uncoated fs laser-machined silicon substrates are 0.2 and 4 mW, respectively. All spectra are recorded with an accumulating time of 10 s.

The SERS spectrum is shown in Fig. 4(a). The legend in Fig. 4(a) indicates the order and type of substrate processing, where Film, NPs, and FS indicate gold coating, gold-coating with thermal dewetting, and fs laser machining, respectively. Therefore, the legend of FS, FS + Film and FS + NPs in Fig. 4(a) correspond to the schematic diagrams of (b), (c), and (d) in Fig. 1, respectively. The legend of the NPs, as shown in the green line in Fig. 4(a), is corresponding to thermal dewetting on a flat surface. From the SERS spectrum, a better quality spectrum is obtained in the case of FS + NPs, as shown by the red line.

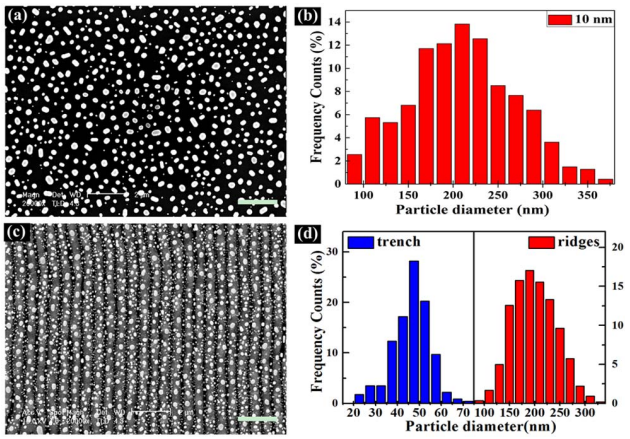

Fig. 3. SEM images of NPs (a) on flat silicon surface and (c) on the ripple structure of 10 nm Au film dewetting; (b) and (d) are size distribution of NPs, respectively.

There is no apparent signal of R6G in the case of NPs on flat silicon, as shown by the green. According to the results, it can be observed that the peak intensities of the Raman signal in the case of FS + NPs are greater than that of the case of NPs. This is due to the light-trapping effect of the ripple structure, which couples the incident photon efficiently to the 3D microstructure to excite the molecules[20]. Meanwhile, the case of FS + Film, shown by the blue line, produces a much weaker signal to the case of FS + NPs. Because of treating with thermal dewetting, the gold film starts to break down and generates abundant "hot spots" (the gap between two individual metal particles) that exhibit a high coupling electric field to enhance the Raman intensity. There are no visible Raman peaks when acquiring the signal in the case of FS, as shown by the black line. We also investigate the uniformity of the SERS intensity of the substrate coated with 10 nm of gold using thermal dewetting. Figure 4(b) shows the Raman mapping of a SERS-active region using the integrated intensity of the 1361 ± 10 cm^{-1} Raman band of R6G. The greatest deviation of the 400 test points is estimated to be in the range of 25%, which is lower than the result in Ref. [15] and demonstrates the highly homogeneous signals. Moreover, the fabricated SERS-active substrate also exhibits excellent chemical stability. The stability of the SERS-active substrate is examined by placing the substrate in the air for a month. The intensity of 1361 cm^{-1} is still close to that of the original prepared substrate with the greatest deviation of 6%. All the EFs are the average values of three substrate samples, and each is measured at 5 different locations.

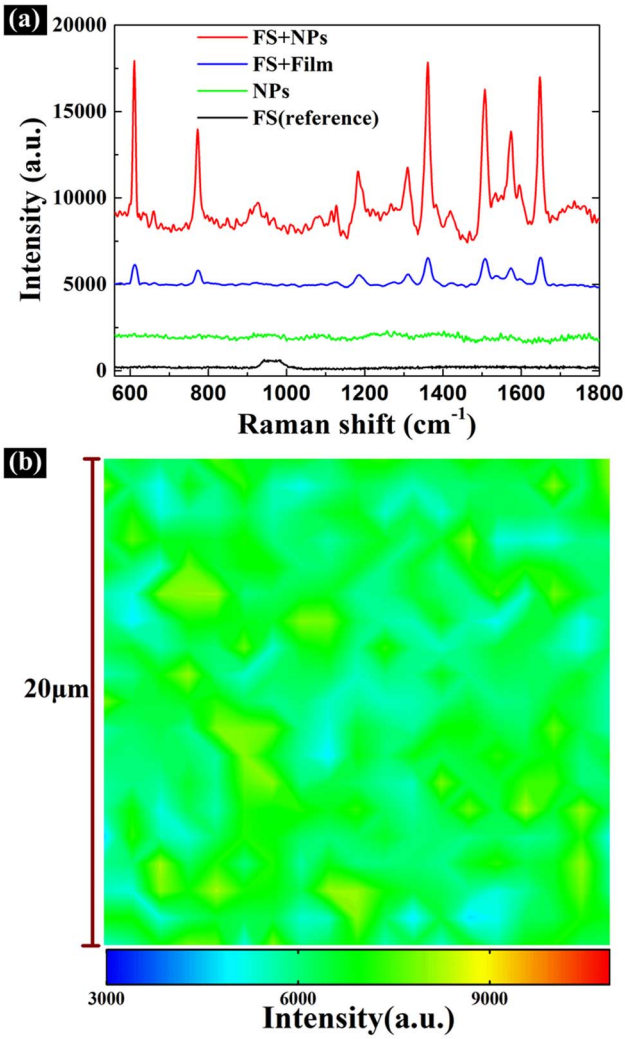

Fig. 4. (a) SERS spectra of different processing substrate. Red: FS+NPs area with 10^{-6} mol/L R6 G; Blue: FS + Film with 10^{-6} mol/L R6G; Green: NPs with 10^{-6} mol/L R6G; Black: fs laser-machined silicon with 10^{-2} mol/L R6G. (b) Raman map image of 20 μm × 20 μm areas on the SERS substrates.

The EFs are evaluated with the equation

$$\mathrm{EF} = \frac{I_{\mathrm{surf}}}{N_{\mathrm{surf}}} \Big/ \frac{I_{\mathrm{vol}}}{N_{\mathrm{vol}}}, \tag{1}$$

where I_{vol} and I_{surf} are the normal Raman and SERS intensities in the units of mW^{-1} s^{-1}, and N_{vol} and N_{surf} represent the number of molecules detected in the reference sample and on the SERS-active substrate, respectively. As the surface roughness of the normal Raman and the SERS substrate are close to each other, it is reasonable to assume that the measured molecules on the normal Raman and the SERS are identical and the EF can be simplified to the ratio of the intensity of SERS and the normal Raman. Calculated by Eq. (1) with the aforementioned assumption and conditions, the EFs at the Raman peak 1361 cm^{-1} are estimated to be 5.2×10^7, demonstrating the high sensitivity.

The influence of Au film thickness on the SERS activity is also studied experimentally (as shown in Fig. 5). The size and spacing of gold NPs strongly affect the LSPR that constitutes the foundation of EM enhancement of SERS[21,22]. From the SEM in Figs. 6(c)–6(e), the NPs sizes are apparent larger than 200 nm on the ridges when the film thickness is greater than 10 nm, hence we believe the attribution of NPs on the ridges to Raman enhancement can be neglected for its larger particle and wider spacing.

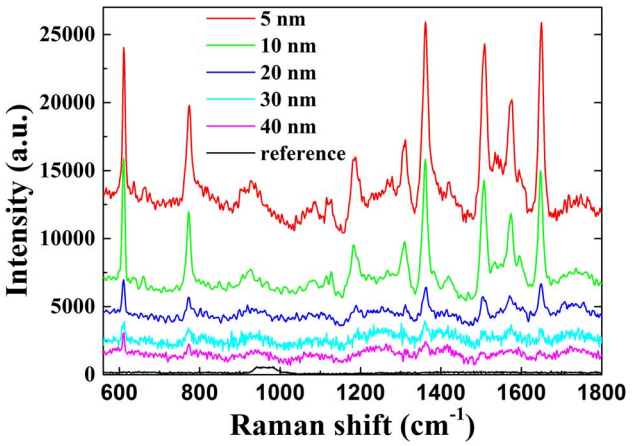

Fig. 5. SERS spectrum on fs laser-machined, gold-coated, thermal dewetting substrates coating different thicknesses of films.

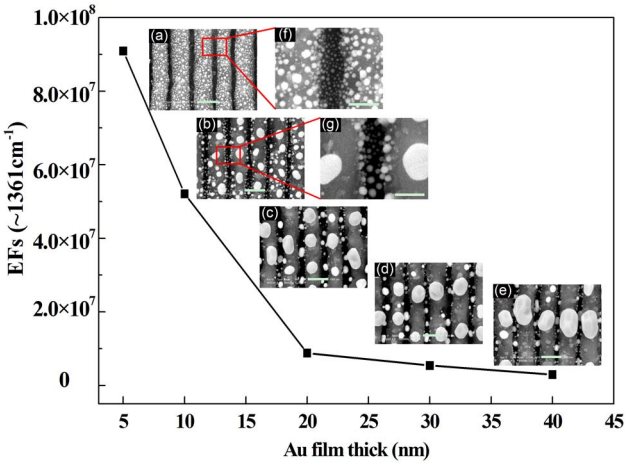

Fig. 6. EFs of SERS signal at 1361 cm^{-1} on fs laser-machined, gold-coated, thermal dewetting substrates coating different thicknesses of gold films. (a)–(e) scale bars represent 500 nm, (f) and (g) represent 200 nm.

The result is shown in Fig. 6; it can be noted that by gradually decreasing the thickness of Au film from 40 to 10 nm, better SERS performance is observed due to that the NP sizes gradually decreasing to about 50 nm in the trench. It has been demonstrated both theoretically and experimentally that an isolated spherical gold NP yields the maximum enhancement when the particle diameter is ~60 nm[23]. When the thickness of Au film is further decreased to 5 nm, the sample exhibited the highest enhancement. Although the particle size of 10 nm film is closer to 60 nm in the trench, the density of NPs has declined rapidly and the spacing of NPs is wider than the film of 5 nm, as shown in Figs. 6(f) and 6(g). The coverage of Au NPs in the trench is approximately 1400 and 400 particle/μm^2 in the film of 5 and 10 nm, respectively. As a consequence, the density of the so-called "hot spots" declines due to the loss of nanogaps, and the SERS performance is adversely affected in the 10-nm film. It is also worthwhile mentioning that, in the film of 20–40 nm, the EFs are quite analogous but lower than that of the 10 nm. The surface coverage of the NPs in the trench is low and their distribution is similar to each other, as shown in Figs. 6(c)–6(e). With larger interparticle spacing, the EFs are approximately constant, which agrees well with the conclusion in Ref. [24]. When the film is thinner than 3 nm it will produce less Au NPs in the trench after dewetting and the EFs decline with instability.

In conclusion, a reliable and cost-effective substrate with large-scale uniformity and high EFs can be obtained by combining fs laser machining, gold coating, and thermal dewetting. The SERS EFs up to 9.2×10^7 are achieved and the greatest deviation of Raman intensity from over 400 test points is in the range of 25%. The chemical stability exhibits a great advantage because the substrate's Raman intensity only varies 6% after it is exposed in the air for a month. Thus, our technique can be attractive as a cost-effective method for fabricating SERS-based biochips or lab-on-a-chip devices with high sensitivity, spatial uniformity, and excellent chemical stability, which will find a broad range of applications in the fields of chemical and biological analyses.

This work was supported by the National 973 Program of China (No. 2011CB013000), the National Natural Science Foundation of China (Nos. 91323301 and 51322511), and the Cultivation Fund of the Key Scientific and Technical Innovation Project, Ministry of Education of China (No. 708018).

References

1. M. Fleischmann, P. J. Hendra, and A. J. McQuillan, Chem. Phys. Lett. **26**, 163 (1974).
2. D. L. Jeanmaire and R. P. Van Duyne, J. Electroanal. Chem. **84**, 1 (1977).
3. A. Campion and P. Kambhampati, Chem. Soc. Rev. **27**, 241 (1998).
4. M. Moskovits, Rev. Mod. Phys. **57**, 783 (1985).
5. C. J. Murphy, A. M. Gole, J. W. Stone, P. N. Sisco, A. M. Alkilany, E. C. Goldsmith, and S. C. Baxter, Acc. Chem. Res. **41**, 1721 (2008).
6. H. Wang, D. W. Brandl, P. Nordlander, and N. J. Halas, Acc. Chem. Res. **40**, 53 (2007).
7. P. J. Liu, L. Jiang, J. Hu, W. N. Han, and Y. F. Lu, Opt. Lett. **38**, 1969 (2013).
8. X. Ji, L. Jiang, X. W. Li, W. N. Han, Y. Liu, A. D. Wang, and Y. F. Lu, Appl. Surf. Sci. **326**, 216 (2015).
9. C. Wang, Z. Luo, J. A. Duan, L. Jiang, X. Y. Sun, Y. W. Hu, J. Y. Zhou, and Y. F. Lu, Laser Phys. Lett. **12**, 056001 (2015).
10. Z. Luo, C. Wang, J. A. Duan, X. Y. Sun, Y. W. Hu, and K. Yin, Appl. Opt. **54**, 3943 (2015).
11. K. Yin, J. A. Duan, X. Y. Sun, C. Wang, and Z. Luo, Appl. Phys. A **119**, 69 (2015).
12. Z. Luo, J. Duan, C. Wang, X. Sun, and K. Yin, Chin. Opt. Lett. **13**, 051403 (2015).
13. Z. Q. Zhu, Z. D. Yan, P. Zhan, and Z. L. Wang, Sci. China Phys. Mech. Astron. **56**, 1806 (2013).
14. E. D. Diebold, P. Peng, and E. Mazur, J. Am. Chem. Soc. **131**, 16356 (2009).
15. C. H. Lin, L. Jiang, J. Zhou, H. Xiao, S. J. Chen, and H. L. Tsai, Opt. Lett. **35**, 941 (2010).
16. A. Hamdorf, M. Olson, C. H. Lin, L. Jiang, J. Zhou, H. Xiao, and H. L. Tsai, Opt. Lett. **36**, 3353 (2011).
17. L. Jiang, D. W. Ying, X. Li, and Y. F. Lu, Opt. Lett. **37**, 3648 (2012).
18. N. Zhang, X. Li, L. Jiang, X. S. Shi, C. Li, and Y. F. Lu, Opt. Lett. **38**, 3558 (2013).
19. Q. Q. Yang, X. Li, L. Jiang, N. Zhang, G. M. Zhang, X. S. Shi, K. H. Zhang, J. Hu, and Y. F. Lu, Opt. Lett. **40**, 2045 (2015).
20. T. W. Chang, M. R. Gartia, S. Seo, A. Hsiao, and G. L. Liu, Nanotechnol. **25**, 145304 (2014).
21. P. P. Fang, J. F. Li, Z. L. Yang, L. M. Li, B. Ren, and Z. Q. Tian, J. Raman Spectrosc. **39**, 1679 (2008).
22. P. N. Njoki, I. I. S. Lim, D. Mott, H. Y. Park, B. Khan, S. Mishra, R. Sujakumar, J. Luo, and C. J. Zhong, J. Phys. Chem. C **111**, 14664 (2007).
23. J. T. Krug, G. D. Wang, S. R. Emory, and S. M. Nie, J. Am. Chem. Soc. **121**, 9208 (1999).
24. Z. H. Zhu, T. Zhu, and Z. F. Liu, Nanotechnology **15**, 357 (2004).